Available online at www.sciencedirect.com
ScienceDirect
Journal of Hazardous Materials 150 (2008) 99–108
Journal of Hazardous Materials
www.elsevier.com/locate/jhazmat

Apatite and Portland/apatite composite cements obtained using a hydrothermal method for retaining heavy metals

M.I. Domínguez [a,*], J. Carpena [b], D. Borschnek [b], M.A. Centeno [a], J.A. Odriozola [a], J. Rose [b]

[a] *Instituto de Ciencia de Materiales de Sevilla, Centro Mixto CSIC-Universidad de Sevilla, Avda, Américo Vespucio s/n 41092 Sevilla, Spain*
[b] *CEREGE UMR 6635 CNRS-université Aix-Marseille III, Europôle de l'Arbois, BP 80, 13 545 Aix en Provence cedex 4, France*

Received 2 October 2006; received in revised form 16 April 2007; accepted 17 April 2007
Available online 24 April 2007

Abstract

Apatite and Portland/apatite composite cements containing steelwork dusts have been prepared using a low temperature hydrothermal method (200° C, 48 h). The produced solids were characterized by means of XRD, IR, and SEM-EDX, and the remaining liquid was analyzed by ICP. The results clearly show the capability of these cements to inertise the heavy metals contained in steelwork dusts, that is Fe, Pb, Mo, Cr, Mn, Ni, and Zn. In the case of apatitic cements, Fe, Mg, Cr, Mn, and Pb coming from steel dust replaced Ca in the divalent cation position of the apatite structure, while Si and Mo replaced P in tetrahedral position. The average crystal size of the apatite-containing dust is smaller than in pure apatite synthesized using the same procedure, which is related to the magnesium content of the dust, since magnesium seems to inhibit the crystal growth. XRD diagrams of composite cements show only peaks corresponding to phases observed in the single cements, and in that no new phases are found. However, EDX analysis reveals the introduction of cations coming from Portland cement into the apatite structure. From the results of water analysis it could be concluded that the capability of retention is higher in composite matrices than in the pure apatite one. In conclusion, the obtained data allow stating that the proposed method, the hydrothermal synthesis of steelwork dust containing cement, is a reliable one for immobilization of toxic residues containing heavy leachable cations.
© 2007 Elsevier B.V. All rights reserved.

Keywords: Immobilization; Heavy metals; Apatite cement; Portland cement; Composite cement

1. Introduction

Industrial processes usually result in the production of by-products and residues. In the case of stainless steel mills, these by-products and residues contains toxic metals. Among the variety of residues produced in stainless steel mills, steel dusts contain toxic, leachable heavy metals and have been catalogued as a dangerous waste.

The use of plasma furnaces for the recycling of stainless steel-making dust is described by Neuschutz [1] and is mostly documented in patents [2,3]. However, plasma processes are costly enough for being usually discarded even in the case of high nickel concentration. Other recovery methods, mostly consisting in high temperature oxide reduction have been proposed [4–6]. If immobilization is taken as an alternative [7,8], the design of matrices that prevent the dispersion of toxic heavy metals like Cr, Ni, Zn, and Pb among others in the environment is of paramount importance for avoiding any environmental risk.

Portland cements and apatite have been described as matrices to inertise industrial wastes. Portland cement is made by heating a mixture of limestone and clay at 1450 °C. After heating, it is milled and mixed with gypsum (calcium sulphate) which allows regulate cement setting. Typical composition of a clinker is: 67% CaO, 22% SiO_2, 5% Al_2O_3, 3% Fe_2O_3, and 3% of other components. In a clinker, calcium silicates form single crystals into a matrix of calcium aluminates and ferroaluminates. Cement is a hydraulic adhesive, addition of water to the cement produces a paste that sets and hardens. The whole phases react with water by dissolution–diffusion–precipitation reactions producing the different hydrated phases. Portland cement admits a percentage of waste into its composition without affecting its characteristics. Several studies have been published on this subject [9,10],

* Corresponding author. Tel.: +34 954489543; fax: +34 954460665.
E-mail address: mleal@icmse.csic.es (M.I. Domínguez).

0304-3894/$ – see front matter © 2007 Elsevier B.V. All rights reserved.
doi:10.1016/j.jhazmat.2007.04.091

showing that Portland cement matrix is adequate for Zn, Cu, Pd, and Cu stabilization, among other metals. Intermediate phases in the system $CaO\text{-}SiO_2\text{-}Al_2O_3$-metal oxide are formed which become stable during clinker formation and/or cement hydration.

Apatites form a large family of isomorphous minerals with the general chemical formula $Me_{10}(XO_4)_6Y_2$, where Me represents a divalent cation, XO_4 a trivalent anionic group and Y, a monovalent anion [11,12]. A well-known representative member of the apatitic family is calcium phosphate fluoroapatite, $Ca_{10}(PO_4)_6F_2$. One of the main characteristics of the apatite structure is the possibility of substituting all of the elements, when the substitution implies elements with different ionic charges it is possible to equilibrate the charge balance. For example, it is possible to prepare a complete series of oxyapatites by the substitution pair $La^{3+} + SiO_4{}^{4-} \leftrightarrow Ca^{2+} + PO_4{}^{3-}$ [13]. The minerals obtained through this substitution are designated as britholites. A clear explanation of the crystallochemistry and substitution possibilities in apatites and britholites can be found in Boyer et al. [14]. In the case of radioactive elements it has been possible to find britholites in the natural nuclear reactor of Oklo without corrosion or irradiation damage [15].

The main properties of the apatite structure are its ability to admit a large number of substitutions, its high chemical stability in geological medium and towards water corrosion in neutral to basic pH and its weak and retrograde solubility. Because of this, apatite has been used in applications like biomaterials [16], chromatography [17], sensors [18], detoxification of wastes and water [19], and for the immobilization of radioactive wastes [20].

Among all of the proposed synthesis methods for obtaining apatite, the hydrothermal treatment is very simple and economical. Mixtures of calcium phosphates, with or without plasticizers, in the presence of water set and harden at room temperature resulting in apatitic cements [21]. Using hydrothermal reactors, the evolution from the powdery to coherent material occurs due to the combined action of physical and chemical phenomena: temperature, pressure, and chemical reactions between constituents, the mechanical properties of the obtained cements depending on the liquid/solid ratio. For example, in apatite cements, the highest mechanical properties are achieved at L/S ratio between 0.4 and 0.45 cm^3/g. In spite of this fact, the hydrothermal method uses water in excess to allow setting and hardening. In order to minimize the effect of this excess of water, the initial powder is pressed before its introduction into the autoclave, producing the particles approaching and the slow diffusion of water through the pellet. In the hydrothermal process all of these reactions occur at temperatures above the liquid boiling point. For temperatures over 100 °C, a part of the water in the reactor vaporizes, rising the internal pressure. At final temperature, the equilibrium between liquid and vapor water is established [22].

The immobilization of hazardous heavy metals, stainless steel-making dusts, in ceramic bodies that meet environmental regulations might benefit of the ability of apatites to accommodate cations and tetrahedral anions within the solid structure, due to their physical (mechanical properties) and chemical (high stability towards water corrosion in neutral to basic pH and weak and retrograde solubility) properties. In this study we prepare ceramic bodies in which the stainless steel-making residues are immobilized in apatite and Portland/apatite composite cements by means of a low temperature hydrothermal method.

2. Materials and methods

Apatite and Portland/apatite composite cements were prepared by a hydrothermal method. The composition of the different prepared samples is shown in Table 1. The apatitic cement was obtained following the formulation of Mejdoubi and Lacout [23]. The reactants, monocalcium phosphate (MCPM, PROLABO Rectapur, purity = 92%), β tricalcium phosphate (Obtained from Apatite type TCP, PROLABO Rectapur, after calcination for 3 h at 900 °C) and tetracalcium phosphate (TTCP, TEKNIMED), were milled together in a mortar until the particle size of the powders was smaller than 50 μm. Two pellets of the mixture (total weight 1.250 g) were prepared in a 10 mm diameter infrared die at 21 MPa and introduced in a hydrothermal reactor with 100 ml of de-ionized water. The reactor is heated in a furnace at 200 °C for 48 h. Once the heating schedule is finished the reactor is allowed to cool down in air to room temperature and the obtained solid is taken away from the reactor and oven-dried at 50 °C. The addition of water to the mixture of calcium phosphates results in the formation of hydroxyapatite (HAp) according to reaction (1).

$$x\mathrm{Ca(H_2PO_4)_2 \cdot H_2O} + (2-3x)\mathrm{Ca_3(PO_4)_2} + (1+2x)\mathrm{Ca_4(PO_4)_2O} \xrightarrow{\mathrm{H_2O}} \mathrm{Ca_{10}(PO_4)_6(OH)_2} \quad (1)$$

This type of formulation, with three components, allows varying the constituent proportions, which affects the physical and chemical properties but always obtaining hydroxyapatite.

Composite matrices have been prepared by adding different quantities of a commercial Portland cement to the calcium phosphate mixture used as precursor of apatite cement. Table 2 shows the chemical composition of the used Portland cement.

Finally, steel dust coming from the stainless steel factory of ACERINOX S.A., placed in Los Barrios (Cádiz, Spain), has been used. Its chemical composition obtained by ICP is showed in Table 3. The XRD analysis indicates that the steel dust is a mixture of highly sinterised metal oxides (Fe_3O_4, Cr_2O_3, Mn_3O_4, ZnO, NiO, MoO_3, $Pb_{12}O_{19}$, CaO, MgO).

Table 1
Composition of the initial mixtures in composite cements

Reference	Composition (% weight)				
	MCPM	β-TCP	TTCP	Portland	Dust
MA1	10.23	24.53	65.24	–	–
MA2	9.21	22.08	58.72	–	10
MAP1	9.21	22.08	58.72	10	–
MAP2	8.70	20.85	55.45	10	5
MAP3	7.68	18.4	48.93	25	–
MAP4	5.12	12.27	32.62	50	–
MAP5	2.56	6.13	16.31	75	–

Table 2
Chemical composition of Portland cement

Elements	SiO_2	Al_2O_3	Fe_2O_3	TiO_2	CaO	MgO
% weight	20.68	4.78	2.89	0.22	63.17	3.60
Elements	SO_3	K_2O	Na_2O	P_2O_5	Lost in combustion	
% weight	2.75	0.57	0.20	0.13	1.29	

Table 3
Chemical composition of the steel dust

Elements	SiO_2	Al_2O_3	Fe_2O_3	MnO	CaO	MgO	Na_2O
% weight	6.22	0.62	21.81	5.78	18.95	7.86	0.52
Elements	K_2O	Cr_2O_3	CuO	NiO	Mo_2O_3	PbO	ZnO
% weight	1.94	13.34	0.31	2.27	6.39	1.14	6.44

3. Results and discussion

3.1. Apatite cements

By mixing the calcium phosphate components according to reaction (1), HAp is obtained. Fig. 1 shows the XRD pattern of the obtained ceramic body (sample MA1), the diffraction lines of the HAp are dominant and only lines of very low intensity corresponding to non-reacted TCP and TTCP are detected. As expected, needle-like crystals are obtained which are responsible for the hardness of the synthesized ceramic. A representative Scanning Electron Microscopy (SEM) image of the well-formed hexagonal HAp needle-like crystals is shown in Fig. 2.

When adding 10% by weight of stainless steel dusts to the three components mixture resulting in HAp crystals, the XRD pattern of the obtained ceramic (MA2) shows, Fig. 3, that the main crystalline phase is also HAp but, in addition to this phase, iron-rich crystalline compounds are also observed. Calcium-iron hydrogenphosphate and magnetite are clearly seen in the XRD pattern of the prepared material. This clearly states that part of the iron compounds present in the stainless steel dust either does not react with the phosphate mixture to give HAp or results in the formation of different phosphate phases.

The addition of steel dust to the phosphate mixture modifies the size and morphology of the HAp crystals that are no longer needle-like. SEM images of samples containing steel dust show HAp crystallites smaller than in pure apatite samples, with a quite different aspect ratio, Fig. 4a. This morphology change must be associated to the incorporation of elements different from calcium present in the steel dust. It has been previously reported that the incorporation of foreign ions into HAp structure affects its crystallinity, morphology, lattice parameters, and stability [24,25]. For instance, the presence of magnesium impedes

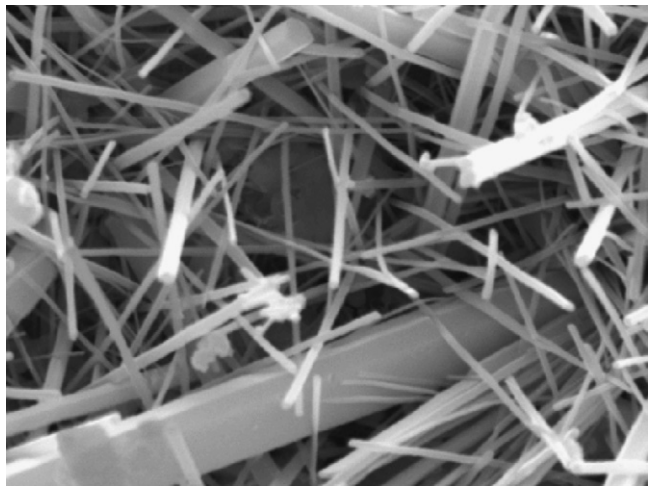

Fig. 2. SEM image of a representative region of the MA1 ceramic body showing formed HAp needle-like crystals of different sizes.

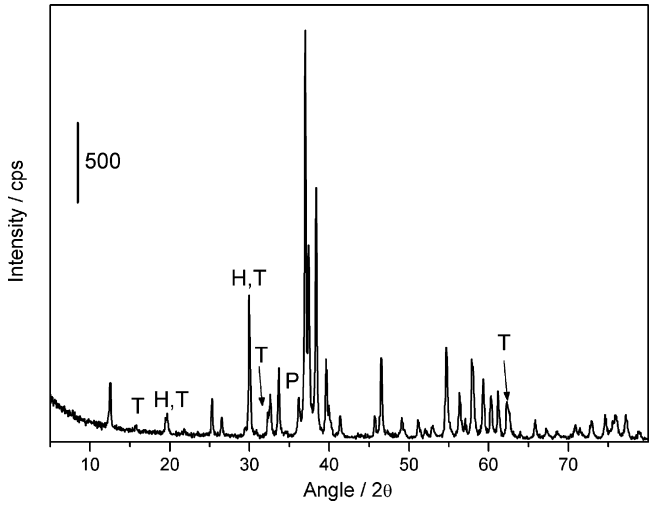

Fig. 1. XRD pattern of the ceramic body obtained after the hydrothermal treatment for sample MA1. All the diffraction lines corresponds to calcium hydroxyapatite, $Ca_5(PO_4)_3(OH)$ marked as H in the figure when overlapping lines corresponding to other crystalline phases, except those marked T (tricalcium phosphate, $Ca_3(PO_4)_2$) or P (tetracalcium phosphate, $Ca_4O(PO_4)_2$).

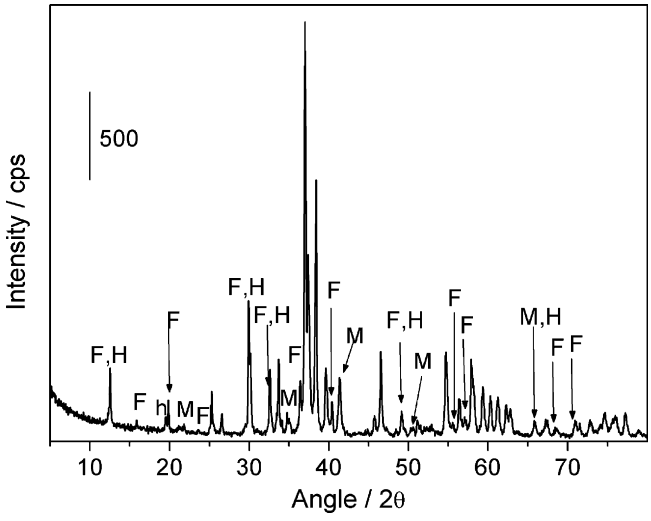

Fig. 3. XRD pattern of the ceramic body obtained after the hydrothermal treatment for sample MA2. All the diffraction lines corresponds to calcium hydroxyapatite, $Ca_5(PO_4)_3(OH)$ marked as H in the figure when overlapping lines corresponding to other crystalline phases, except those marked F (calcium-iron hydrogenphosphate, $Ca_9FeH(PO_4)_7$) or M (magnetite, $FeFe_2O_4$).

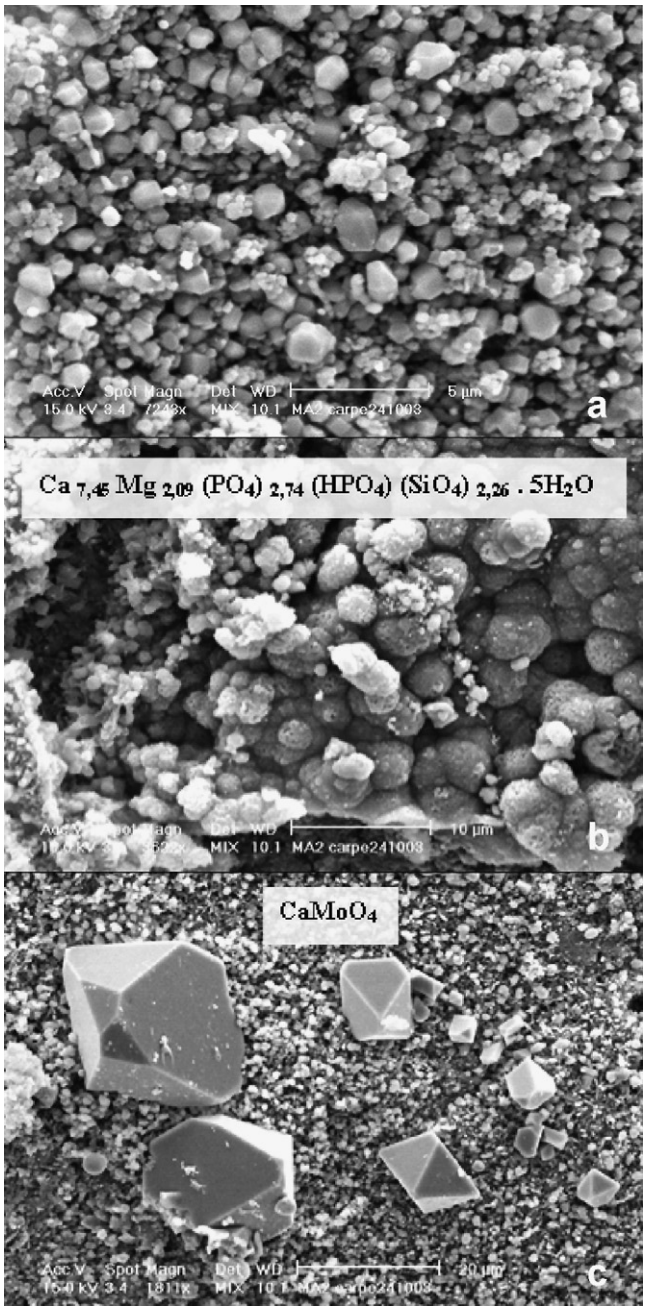

Fig. 4. SEM image of representative regions of the MA2 ceramic body showing: (a) formed HAp rounded crystals of different sizes, (b) octocalcium phosphate, and (c) octahedral powellite crystals.

the crystalline growing, as reported by some authors [41–43]. In addition to the hydroxyapatite crystals, the presence of octocalcium phosphate ($Ca_8(PO_4)_4(HPO_4)_2.5H_2O$) and powellite ($CaMoO_4$) have been found by SEM (Fig. 4b and c, respectively) in sample MA2, although they are not detected by XRD, indicating the low concentration of these phases in the final material. Structural formulas have been obtained from EDX analyses and are included within the figure. Octocalcium phosphate has been suggested as intermediate phase in apatite formation [26], while formation of powellite seems to indicate a reaction between free Mo and Ca coming from steel dust, since it cannot be produced

Table 4
Structural formulas obtained from EDX for several crystals in sample MA2

$Ca_{7,70}\ Mg_{0,48}\ Cr_{0,07}\ Fe_{0,17}\ Pb_{0,24}\ (SiO_4)_{0,11}(MoO_4)_{4,25}(PO_4)_{1,62}(OH)_{1,96}$
$Ca_{8,70}\ Mg_{0,45}\ Fe_{0,09}\ Pb_{0,21}\ \square_{0,55}\ (SiO_4)_{0,1}(MoO_4)_{2,74}(PO_4)_{3,16}(OH)_2$
$Ca_{9,81}\ Mg_{0,4}\ Cr_{0,06}\ Fe_{0,09}\ Pb_{0,08}\ (SiO_4)_{0,1}(MoO_4)_{0,44}(PO_4)_{5,47}(OH)_{1,74}$
$Ca_{9,15}\ Mg_{0,28}\ Cr_{0,06}\ Mn_{0,06}Fe_{0,11}\ Pb_{0,22}\ \square_{0,12}\ (SiO_4)_{0,1}(MoO_4)_{2,74}(PO_4)_{3,16}(OH)_2$
$Ca_{9,67}\ Mg_{0,38}\ Cr_{0,06}\ Mn_{0,05}Fe_{0,3}\ Pb_{0,17}\ \square_{0,12}\ (SiO_4)_{0,1}(MoO_4)_{1,14}(PO_4)_{4,74}\ (OH)_2$

when the amount of available calcium, in the form of $Ca(OH)_2$, is low.

The reaction of the components of steel dust with the calcium phosphates resulting in the partial substitution of both Ca and $(PO_4)^{3-}$ ions by the elements present in the steel dust is stated by EDX chemical analysis of the formed crystals. Table 4 shows the composition of some of these crystals. However, EDX analysis can only be considered as semiquantitative since the presence of carbon, that should accounts for phosphate substitution by carbonates, or hydrogen coming from more acidic environments as, for instance, $(HPO_4)^{2-}$ cannot be considered. As both, hydrogenphosphate and carbonate groups, imply a change in the total charge of the apatitic framework, this must be compensated by the presence of either vacancies or modifications in the total amount of cations entering the calcium hydroxyapatite structure.

The IR spectra of both samples, MA1 and MA2 (Fig. 5a), present the characteristic bands of hydroxyapatite [27,28]. According to Fowler [29], the bands at 3570 and 634 cm^{-1} are assigned to the OH stretching and librational modes in the HAp structure, respectively. A group of weak intensity bands in the 2200 to 1950 cm^{-1} region, not shown in the figure, derives from overtones and combinations of the ν_3 and ν_1 PO_4 modes. In the case of highly crystalline hydroxyapatite, bands at 1091 and the doublet at about 1043 cm^{-1} were assigned to components of the triply degenerate ν_3 antisymmetric PO stretching mode; the 960 cm^{-1} band was assigned to ν_2, the nondegenerate PO symmetric stretching mode. The bands at 603, 578, and 568 cm^{-1}, were assigned to components of the triply degenerate ν_4 OPO bending mode [29]. In addition to these bands, the MA1 ceramic shows bands at 1142 cm^{-1} whose ascription is slightly controversial. While Gadaleta et al. [30] attribute this band to PO_4 vibrations in an apatitic environment of poorly crystalline hydroxyapatite, most of the authors associate this band to the presence of HPO_4^{2-} groups in nonstoichiometric HAp or to the existence of calcium phosphate phases more acidic than HAp as TCP, OCP, DCPD or DCPA [31,32]. The presence of TCP and OCP in both MA1 and MA2 ceramics is stated by XRD and SEM-EDX analysis, which supports the ascription of this band to HPO_4^{2-} vibrational modes.

Upon addition of the steel dust, sample MA2, this general spectrum is slightly modified. Bands in the 1400–1500 cm^{-1} region due to stretching vibrations of carbonate species appear. These peaks are indicative of carbonate apatites. Two peaks can be distinguished in this region at around 1420 and 1464 cm^{-1}

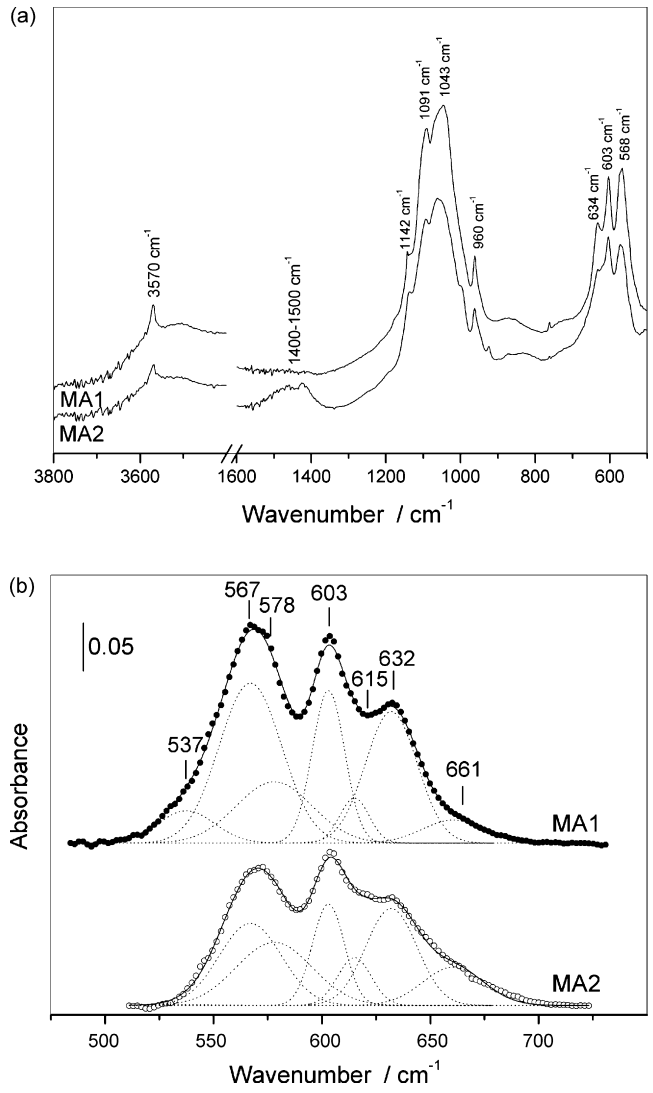

Fig. 5. (a) FTIR spectra of MA1 and MA2 ceramics; (b) Infrared spectra of the ν_4 OPO bending mode of phosphate groups for MA1 and MA2 ceramics showing the different components after deconvolution.

that, in addition to the small peak at 871 cm^{-1}, have to be ascribed to carbonate ions replacing phosphate groups in hydroxyapatite [33,34].

The doublet at 1040 cm^{-1} shifts to higher wavenumbers peaking at 1062 cm^{-1}. This shift must be associated to the interaction of calcium, silicate, and phosphate groups. This ascription is consistent with the results obtained by Sahai and Tosell [35] using molecular orbital calculations of model clusters. In the case of $[Si_3O_6H_5CaHPO_4(H_2O)_3]^-$ cluster, the P–O stretching mode shifts to 1060 cm^{-1} with respect to the doublet at 1040 cm^{-1}. This shift, in addition to the band at 924 cm^{-1}, clearly indicates the presence of silicate ions in the apatite network, since the 924 cm^{-1} band must be ascribed to the ν_3 mode of silicate anions in britholites. [14].

The relative intensity of the peaks at 567 and 603 cm^{-1} changes upon addition of the stainless steel dust in such a way that the intensity ratio between the 567 and 603 cm^{-1} peaks decrease upon addition of the stainless steel dust. This must be associated to a decrease in the crystallinity of the hydroxyapatite upon addition of the steel dust.

In general, the low site symmetry of the PO_4^{3-} tetrahedron splits the triply degenerate ν_4 OPO bending mode into three components. In synthetic and biological apatites, a broad band centered between 530 and 540 cm^{-1} has also been observed being assigned to HPO_4^{2-} groups but also to O–P–O bend in DCPD [35,36]. The intensity of these peak increases as crystallinity of apatite decreases while decreasing the peak intensities at 563, 575, and 603 cm^{-1} [32]. Similarly, the small band at 615 cm^{-1} has to be assigned to P–O and O–P–O stretching and bending modes of phosphate groups in OCP and/or TCP materials [31].

If the IR spectra is deconvoluted in the 450–750 cm^{-1} region, bands at 567, 578, 603, 615, 632, and 661 cm^{-1} and, in the case of the MA1 sample, an additional band at 537 cm^{-1} are observed, Fig. 5b. The substitution in the pure apatite matrix results in the elimination of the band at 537 cm^{-1}. The increasing band at 661 cm^{-1} has to be assigned to H_2O librational mode of dicalcium phosphate dihydrate, $CaHPO_4{\cdot}2H_2O$, (brushite) [37] indicating the existence of HPO_4^{2-} groups upon addition of stainless steel dusts.

In addition to this, it is clear that the intensity ratio between the 603 and 567 cm^{-1} bands increases on increasing the amount of calcium and phosphorous substitution which, according to the early work of Termine and Posner [38], should be associated to a decrease in the apatite crystallinity.

All the obtained data clearly indicate that substitution of calcium and phosphorous in the apatite network took place upon the addition of stainless steel dust. Metals coming from steel dust have entered in the apatite structure, taking the place of calcium (Mg, Mn, Cr, Fe, Pb) and phosphorous (Si, Mo).

Due to their ionic sizes, it is generally accepted that silicon substitutes for P site, via precipitation methods [39], and exists as silicate ion, while magnesium ion substitutes for Ca site, by a dissolution–precipitation mechanism [19], and exists as a magnesium ion [40]. The amount of magnesium substituting calcium ranges from 0.55 to 0.92% which is in accordance with the limited substitution reported by other authors always lower than 1% [41]. Kim et al. [44] reported that 1.97 wt% Si may be introduced in hydroxyapatite structure. However, when co-substitution with magnesium occurs, Si-substitution into hydroxyapatite structure was limited to 1.05 wt%. It was evidenced by XRD analysis at different sintered temperatures. In our case a similar effect is observed since for Mg values close to one, only 0.25 wt% of silicon is incorporated into the HAp structure, while for values of magnesium below 0.5 wt%, up to 0.70 wt% of silicon can be incorporated into the apatite structure.

There are no available data for heavy metal substitutions, in this sense only the formation of volatile molybdenum oxides species after ion implantation has been reported, but in reaction conditions far away from those used in this work [45].

Following the reaction scheme proposed in Eq. (2) some of the OH groups of the HAp structure would be lost to retain charge balance to compensate for the extra negative charge of the silicate groups [39,46], and hence a reduction on the intensity of IR bands corresponding to OH groups must be observed. In

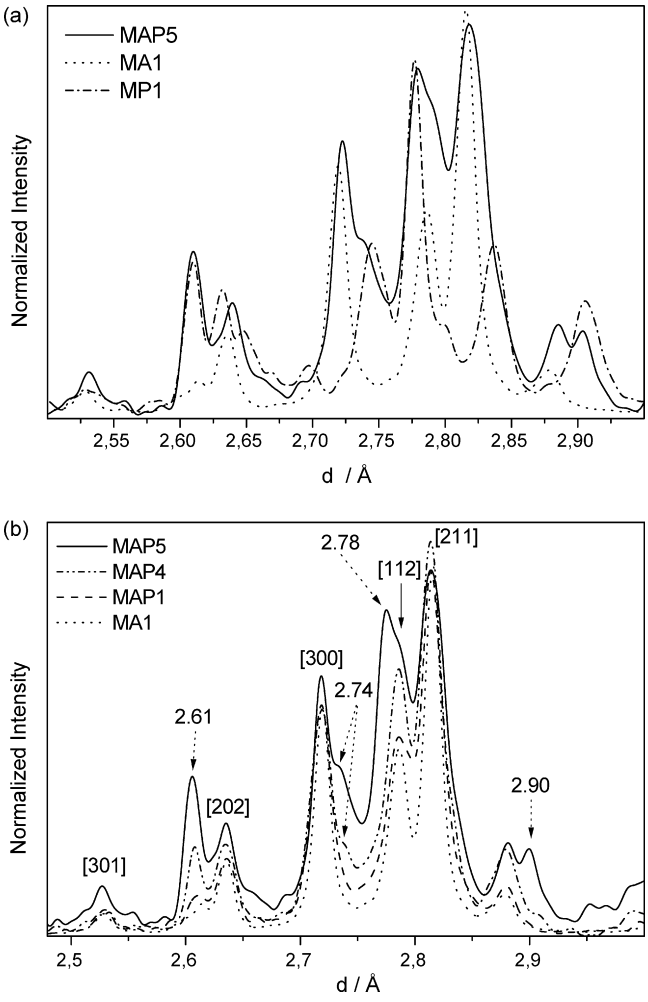

Fig. 6. XRD patterns of the prepared cements.

Fig. 5a is evident a decrease in the relative intensity of the OH stretching band at 3570 cm^{-1} as well as in the OH librational mode at 634 cm^{-1}:

$$10Ca^{2+} + (6\text{-}x)PO_4^{3-} + xSiO_4^{4-} + (2\text{-}x)OH^- \rightarrow Ca_{10}(PO_4)_{(6\text{-}x)}(SiO_4)_x(OH)(2\text{-}x) \quad (2)$$

3.2. Portland/apatite composite cements

The XRD patterns of composite cements are complex showing crystalline phases resulting from the hydrothermal treatment of the Portland cement together with apatite phases. Tricalcium silicate (Ca_3SiO_5), dicalcium silicate hydrate ($Ca_2SiO_4{\cdot}nH_2O$), jaffeite ($Ca_6(Si_2O_7)(OH)_6$), portlandite ($Ca(OH)_2$) and brownmillerite ($Ca_2(Al,Fe)_2O_5$) are identified in the composite ceramics. In Fig. 6a the XRD of the composite made with the higher proportion of Portland cement (MAP5) is shown. It is clear that this diffraction pattern can be interpreted as the linear combination of the one corresponding to the hydroxyapatite phase (MA1) and the phases resulting from the hydrothermal treatment of the Portland cement (MP1). Fig. 6b shows the XDR patterns of the composite cement as a function of the Portland cement added. On increasing the amount of Portland cement it is clear that the intensity increase of the peaks at 2.90 (jaffeite), 2.78 (tricalcium silicate and brownmillerite), 2.74 (tricalcium silicate and dicalcium silicate hydrate), and 2.61 Å (jaffeite). The presence of portlandite (not shown in the figure) is also evidenced by the presence of a peak at 3.11 Å whose intensity also increases on increasing the proportion of Portland cement. However, the presence of phases resulting from the interaction of the two different cements cannot be observed. Despite of this, the hydrothermal treatment of these mixture favors the replacement of calcium and phosphorous by elements present in the Portland cement. Fig. 7 shows a secondary electron image of the MAP1 ceramic showing interlaced hydroxyapatite needles. The EDX analyses of these needles clearly states that some elements coming from Portland cement have entered in the structure of the apatite, in calcium (Mg, Al y Fe), phosphorus (Si y S), and OH (Cl) positions. The structural formulas calculated for selected crystals of apatite formed in sample MAP1 are shown in Table 5. On increasing the percentage of Portland cement the morphology of crystallites changes, appearing now, in addition to needle-like structures, platelets and particles without defined morphologies, although the needle-like particles correspond now to calcium silicates instead of corresponding to hydroxyapatite crystals. The chemical composition of the formed silicates affects the growth habit of the crystals, thus for Ca/Si ratios between 3 and 4 needles are formed, whereas bricks-like crystal are formed when this ratio ranges between 2 and 3, Fig. 8. In addition to this, crystals of jaffeite and portlandite are clearly seen within the obtained ceramics.

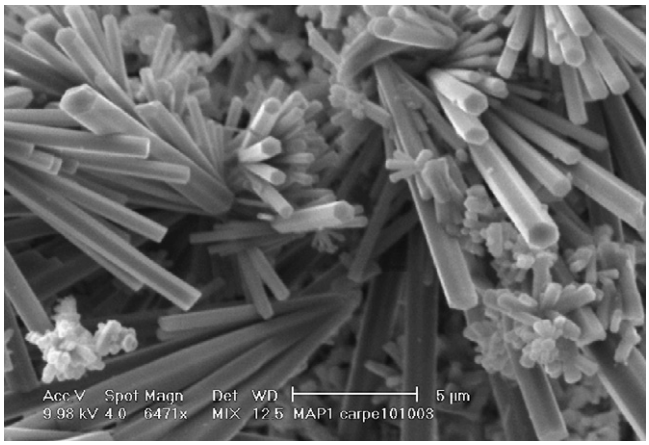

Fig. 7. SEM image of sample MAP1 (hydroxyapatite).

The mixture of crystalline phases observed by XRD and SEM-EDX is also observed using FTIR, Fig. 9. The IR spectra show peaks at 3695, 3640, and 3570 cm^{-1} corresponding to OH stretching modes assigned to Al–OH stretching in aluminates

Table 5
Structural formulas obtained for MAP1 using EDX analysis

$Ca_{9,28}\ Mg_{0,19}\ Al_{0,04}{}^{\square}{}_{0,49}\ (SiO_4)_{0,14}(SO_4)_{0,22}(PO_4)_{5,63}(OH)_{1,02}Cl_{0,15}$
$Ca_{9,56}\ Mg_{0,16}\ Al_{0,06}\ Fe_{0,16}{}^{\square}{}_{0,03}\ (SiO_4)_{0,24}(SO_4)_{0,29}(PO_4)_{5,46}(OH)^{1,6}Cl_{0,10}$
$Ca_{9,82}\ Mg_{0,15}\ Al_{0,06}\ (SiO_4)_{0,10}(SO_4)_{0,23}(PO_4)_{5,68}(OH)_{2,2}Cl_{0,02}$

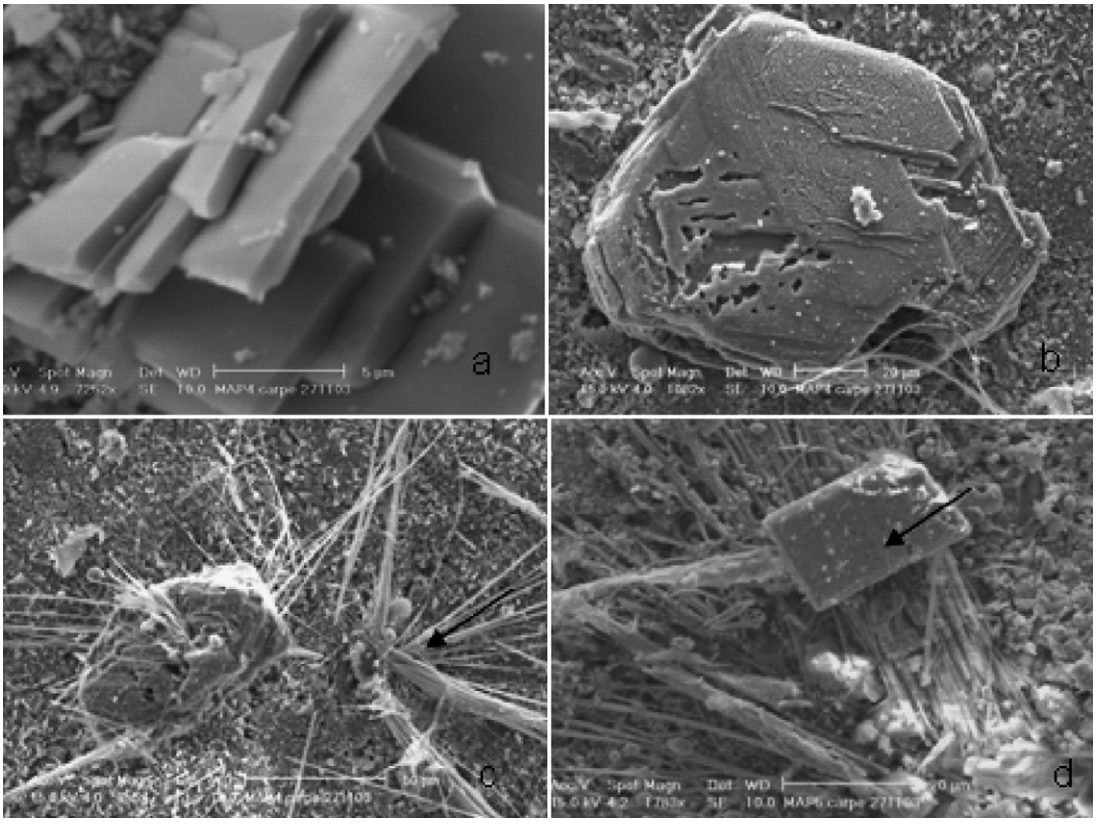

Fig. 8. SEM images corresponding to samples MAP3 and MAP4: (a) Jaffeite, (b) Portlandite, (c) Calcium silicate Ca/Si = 3–4 y d) calcium silicate Ca/Si = 2–3.

[47], OH stretch in portlandite [48] and OH stretching modes in hydroxyapatite [29], respectively. The presence of carbonate substituting phosphate in the apatite structure is evidenced, as in the case of the apatitic ceramics, by the bands in the 1400–1500 cm^{-1} region and the band at 875 cm^{-1}. Calcium silicates, dicalcium (C_2S), and tricalcium (C_3S), present bands corresponding to Si–O modes at 943 cm^{-1} for C_3S and 875 and 834 cm^{-1} for C_2S. As discussed above the bands at 1091 and 1052 cm^{-1} were assigned to components of the triply degenerate ν_3 antisymmetric PO stretching mode; and the one at 960 cm^{-1} is assigned to ν_2, the nondegenerate PO symmetric stretching mode of HAp phases. The HAp show bands at 603 and 568 cm^{-1} corresponding to the ν_4 bending mode of O–P–O bonds, while the band at 634 cm^{-1} is ascribed to the librational OH mode in hydroxyapatite. Finally, the ascription of the band at 1143 cm^{-1} is again controversial. It could be ascribed either to HPO_4^{2-} vibrational modes, or to Si–O stretching vibration of Q4 units (SiO_4 tetrahedra with 4 bridging oxygens) [49] or to the ν_3 mode of sulphate [48].

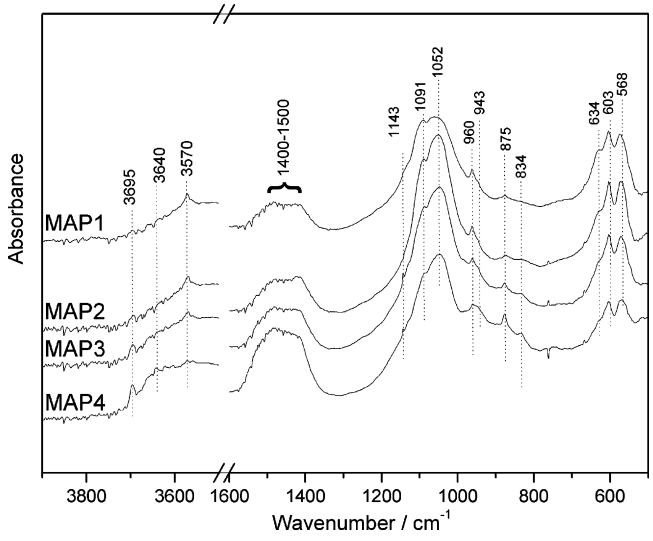

Fig. 9. IR spectra of composite ceramics.

On diminishing the relative proportion of the calcium phosphates with respect to Portland cement, the band corresponding to the OH stretching modes of $Ca(OH)_2$ and aluminates increase their intensities, while the one at 3570 cm^{-1} decreases its intensity. This has to be understood as a decrease in the relative proportion of HAp with respect to the hydrated cement phases as stated by XRD. At the same time the bands corresponding to C_3S and C_2S increase on increasing the proportion of Portland, remaining almost unchanged the rest of the bands. This points to the assignment of the 1143 cm^{-1} band to the stretching modes of S–O in sulphate groups replacing phosphate in the apatite, since the degree of substitution remains within the experimental error for all the samples studied, Table 5. At the same time, as in the case of the apatitic cement, the librational OH mode decreases on increasing the proportion of Portland which clearly suggests that silicate ions are replacing phosphate groups according to Eq. (2). Besides this, the relative intensity of the bands at 603 and

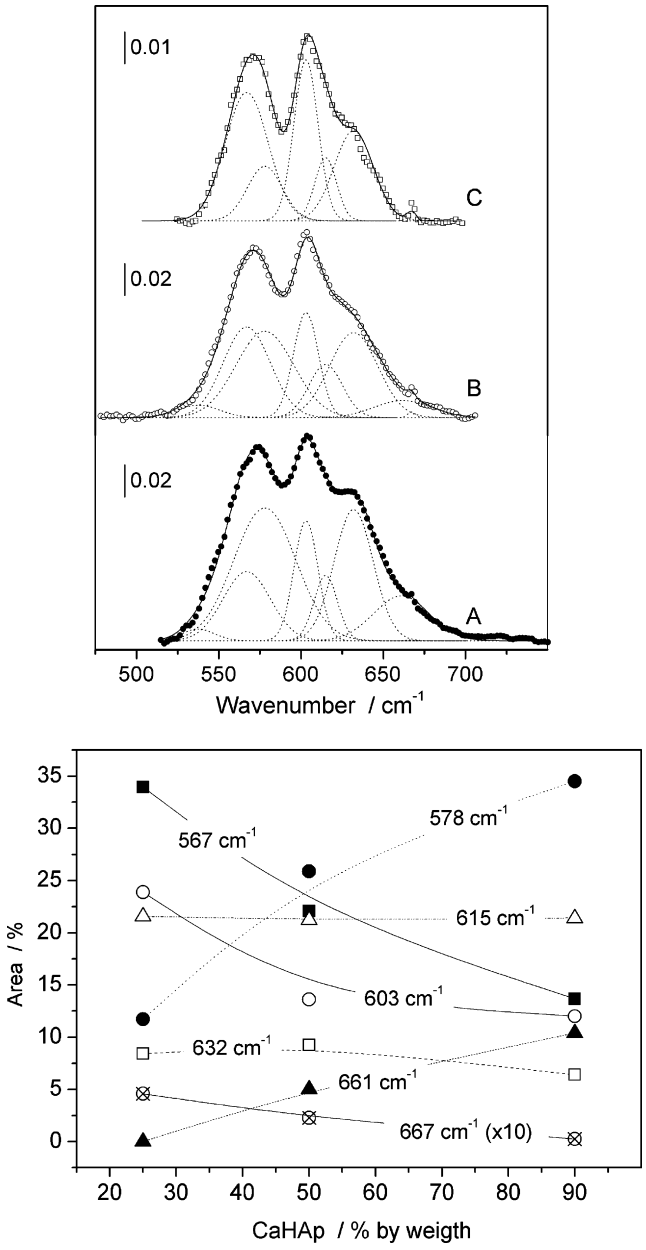

Fig. 10. Top panel: Infrared spectra of the ν_4 OPO bending mode of phosphate groups for MAP ceramics showing the different components after deconvolution. (a) MAP1, (b) MAP4, and (c) MAP5; Bottom panel: Evolution of the relative area under the band components of the ν_4 O—P—O bending mode of phosphate groups for MAP ceramics as a function of the theoretical content of HAp ceramic.

568 cm^{-1} changes monotonically upon the addition of Portland cement.

In order to understand the modifications of the line shape observed upon addition of Portland cement, the IR spectra of materials prepared by increasing the proportion of the Portland cement were deconvoluted, Fig. 10 (top panel). Except for the sharp band at 667 cm^{-1}, that only appears upon addition of the Portland cement, the IR spectra of the obtained material in the 450–750 cm^{-1} region are dominated by the same bands already observed in the CaHAp spectrum, Fig. 5b. However, after an appropriate curve fitting analysis of the spectra, some clear trends are observed, Fig. 10 (bottom panel). Three groups of bands can be distinguished; the first one includes bands whose intensity increase on increasing the percentage of Portland cement added (567, 603, and 667 cm^{-1}); the second one in which the intensity decrease on increasing the amount of Portland cement (578 and 661 cm^{-1}) and the third one which includes the remaining bands, that does not change their intensities as a function of the modification with Portland cement. These bands cannot be ascribed to vibrational modes associated directly to [SiO_4] structural units, but to vibrational modes of phosphate groups affected by the presence of silicate anions. As the bands whose intensity increase are associated to more acidic phosphate species, the possibility of compensating the unbalanced charge in the apatite structure by substituting PO_4 groups by SiO_4 groups is the protonation of one phosphate group for every silicate introduced in the apatite network, as schematized in Eq. (3). This substitution would reduce the stability of the hydroxyapatite network as previously reported [44].

$$10Ca^{2+} + (6\text{-}x)PO_4^{3-} + xSiO_4^{4-} + OH^- + H_2O \rightarrow Ca_{10}(PO_4)_{(6\text{-}2x)}(HPO_4)_x(SiO_4)_x(OH)_2 \quad (3)$$

The addition of a small amount of steel dusts, 5% by weight, to the composite ceramic does not alter either the XRD or the IR spectra except for the presence of a quite small diffraction peak corresponding to magnetite. However, the extremely small size of the HAp crystals, that prevents any analysis by EDX, strongly suggests that most of the metallic cations have entered the hydroxyapatite structure.

3.3. Analysis of reaction water

From the steel dust composition (Table 3), the concentration of each metal in reaction water (assuming that total leaching occurs) can be obtained. By comparison with the real leaching values (obtained by ICP analysis of the water), the percentage of each metal retained by every type of matrix has been calculated (Table 6). As the results show, most of the elements (Mg, Fe, Mn, Cu, Ni, Pb, and Zn) have been retained by both matrices in percentages over 96%. Silicon is retained in a bigger percentage in the matrix containing Portland cement, while aluminium and

Table 6
Percentage of each metal retained by the matrices

Element	% retained by apatite	% retained by composite (10.5% Portland, 89.5% apatite)
SiO_2	56.62	98.35
Al_2O_3	74.53	58.67
Fe_2O_3	100	100
MnO	100	100
CaO	99.41	69.28
MgO	98.91	99.96
Cr_2O_3	96.5	97.16
CuO	99.48	99.64
NiO	100	99.94
Mo_2O_3	59.24	96.7
PbO	99.58	99.12
ZnO	99.99	99.99
Average	90.36	93.23

calcium are retained in higher quantities into the apatite matrix. Molybdenum is almost totally retained in composite matrices, while in apatite its retention is over 60%. This lower retention of molybdenum into the apatite matrix could be explained by the presence of powellite crystals ($CaMoO_4$) in the apatite sample with steel dust. Powellite is formed by reaction between Ca and Mo but, because of absence of enough free calcium, not all the molybdenum has reacted. Finally, composite cement presents the biggest average retention, which could indicate a synergic effect between apatite and Portland cement.

4. Conclusions

Using a hydrothermal method at 200 °C, it has been possible to retain a hazardous waste, with high heavy metals contents, into two different types of cement: apatite and composite Portland/apatite.

The results showed that:

- Pure apatite presents well-formed hexagonal crystals. When steel dust is added, metals enter in divalent cation position (Fe, Mg, Cr, Mn, Pb) as well as in trivalent anionic group position (SiO_4, MoO_4). This apatite presents a very little grain size due to the presence of magnesium in steel dust that impedes the growth of crystal.
- In Portland/Apatite composite mixtures, with 10, 25, 50, and 75% of Portland, apatite is formed as XRD analysis confirms. EDX analysis reveals the introduction of cations coming from Portland cement into the apatite structure. Apatite crystals are small because of the presence of magnesium in Portland cement.
- In composite samples containing steel dust, XRD analysis confirms apatite formation, but again magnesium impedes the crystal growing.
- Reaction water has been analyzed by ICP, showing that metals are retained in a high percentage into both types of matrices. The highest retention is achieved with the composite matrix, which seems to indicate a synergic effect between both materials. Among heavy metals, only molybdenum presents a lower percentage of retention (60%) in apatite matrix. It could be due to the lack of free calcium to react with molybdenum. In this sense, the addition of extra calcium to the initial mixture could improve molybdenum retention.

Acknowledgements

Financial support for this work has been obtained from the Spanish-French "acción integrada Picasso" (HF2003-0247) and Ministerio de Ciencia y Tecnología, MCYT (REN2000-0517). M.I.D. thanks the Spanish Ministerio de Ciencia y Tecnología for the fellowship awarded. Finally, the authors thank ACERINOX S.A. for the supply of stainless steels solid wastes.

References

[1] D. Neuschutz, Plasma processing of dusts and residues, Pure Appl. Chem. 68 (1996) 1159–1165.
[2] S.V. Dighe, W.A. Morgan, J.L. Penland, Process for recovering metals from iron oxide bearing masses, US Patent no. 5728193, 1998.
[3] J.K. Tylko, Treatment of matter in low temperature plasmas, US Patent no. 4394162, 1983.
[4] G.E. Hoffman, J.M. McClelland Jr., Method of producing a metallized briquette, US Patent no. 6802886, 2004.
[5] P. Verdier, J. Rocherulé, Y. Laurent, J. Razafindrakoto, J. Botella, J.A. Odriozola, Procédé d'inertage et de valorisation de déchets, French Patent no. Fr 95 09519, 1995.
[6] J.A. Odriozola, P. Verdier, J.M. Turmel, J. Razafindrakoto, Y. Laurent, Recovering of Metals from Solid Wastes by Redox Processes, in: K.E. Spear (Ed.), Glass Molten Media In: High Temperature Materials Chemistry IX, The Electrochemical Society, Pennington N.J, 1997, p. 288.
[7] E.A. Domínguez, R. Ullman, Ecological bricks made with clays and steel dust pollutants, Appl. Clay Sci. 11 (1996) 237.
[8] D. Tokushuko, Treatment of steel dust to aggregate it - involves mixing with aq. sulphide soln. to form paste, which when solidified can be used for land fill, Japanese Patent no. JP60011254-A, 1985.
[9] J.M. Díez, J. Madrid, A. Macías, Characterization of cement-stabilized Cd wastes, Cem. Concr. Res. 27 (4) (1997) 479–485.
[10] S. Asavapisit, G. Fowler, C.R. Cheeseman, Solution chemistry during cement hydratation in the presence of metal hydroxide wastes, Cem. Concr. Res. 27 (8) (1997) 1249–1260.
[11] T.S.B. Narasaraju, D.E. Phebe, Some physico-chemical aspects of hydroxylapatite, J. Mater. Sci. 31 (1996) 1–21.
[12] J.C. Elliot, Structure and Chemistry of the Apatites and Other Calcium Orthophosphates, Elsevier, 1994.
[13] J. Carpena, L. Boyer, M. Fialin, J.R. Kienast, J.L. Lacout, Ca^{2+}, ${PO_4}^{3-} \leftrightarrow Ln^{3+}$, ${SiO_4}^{4-}$ coupled substitution in the apatitic structure: stability of the mono-silicated flour-britholite, C.R. Acad. Sci. Paris A 333 (2001) 373.
[14] L. Boyer, J. Carpena, J.L. Lacout, Synthesis of phosphate-silicate Apatites at atmospheric pressure, Solid State Ionics 95 (1997) 121–129.
[15] R. Bros, J. Carpena, V. Sere, A. Beltritti, Occurrence of Pu and fissiogenic REE in hydrothermal Apatites from the fossil nuclear reactor 16 at Oklo (Gabon), Radiochim. Acta 74 (1996) 277–282.
[16] N.O. Engin, A.C. Tas, Manufacture of macroporous calcium hydroxyapatite bioceramics, J. Eur. Ceram. Soc. 19 (1999) 2569–2572.
[17] H. Narita, Y. Takeda, K. Takagaki, T. Nakamura, S. Harata, M. Endo, Identification of glycosaminoglycans using high-performance liquid chromatography on a hydroxyapatite column, Anal. Biochem. 232 (1) (1995) 133–136.
[18] M. Nagai, T. Nishimo, T. Saeki, A new type of carbon dioxide gas sensor comprising porous hydroxyapatite ceramics, Sens. Actuators 15 (2) (1988) 145–151.
[19] T.A. Ionannidis, A.I. Zouboulis, Detoxification of a highly toxic lead-loaded industrial solid waste by stabilization using Apatites, J. Hazard. Mater. B97 (2003) 173–191.
[20] J. Carpena, B. Donazzon, E. Céraulo, S. Prené, Élaboration de ciments apatitiques, composites pour la rétention du césium et de l'iode, C.R. Acad. Sci. Paris C 4 (2001) 301.
[21] J. Carpena, B. Donazzon, J.L. Lacout, M. Freche, J Lacout, Production of Apatite ceramics, especially for biomedical use by hydrothermal treatment of compacted calcium phosphate powder mixture at relatively low temperature, Patent no. WO9933766-A;1999.
[22] B. Donazzon, G. Dechambre, J.L. Lacout, Calcium-strontium hydroxyapatite: Hydrothermal preparation, Ann. Chim.-Sci. Mat. 23 (1998) 53.
[23] E. Mejdoubi, J.L. Lacout, M. Hamad, Preparation of calcium phosphate bioceramics by moulding and sintering, Bioceramics 8 (1995) 457–460.
[24] A. Bigi, E. Foresti, A. Ripamonti, N. Roveri, Fluoride and carbonate incorporation into hydroxyapatite under condition of cyclic ph variation, J. Inorg. Biochem. 27 (1) (1986) 31–39.
[25] A. Bigi, M. Gandolfi, M. Gazzano, A. Ripamonti, N. Roveri, A. Thomas, Structural modifications of hydroxyapatite induced by lead substitution for calcium, J. Chem. Soc., Dalton Trans. 11 (1991) 2883–2886.
[26] S. Graham, P.W. Brown, Reactions of octocalcium phosphate to form hydroxyapatite, J. Cryst. Growth 165 (1–2) (1996) 106–115.

[27] H. Zhang, Y. Yan, Y. Wang, S. Li, Thermal stability of hydroxyapatite whiskers prepared by homogenous precipitation, Adv. Eng. Mater. 4 (12) (2002) 916–919.
[28] M. Vallet-Regí, L.M. Rodríguez-Lorenzo, A.J. Salinas, Synthesis and characterisation of calcium deficient Apatite, Solid State Ionics 101–103 (1997) 1279–1285.
[29] B.0. Fowler, Infrared studies of Apatites I. Vibrational assignments for calcium, strontium, and barium hydroxyapatites utilizing isotopic substitution, Inorg. Chem. 13 (1) (1974) 194–207.
[30] S.J. Gadaleta, A. Gericke, A.L. Boskey, R. Mendelsohn, Two-dimensional infrared correlation spectroscopy of synthetic and biological Apatites, Biospectroscopy 2 (6) (1996) 353–364.
[31] S. Koutsopoulos, Synthesis and characterization of hydroxyapatite crystals: A review study on the analytical methods, J. Biomed. Mater. Res. 62 (4) (2002) 600–612.
[32] L.M. Miller, V. Vairavamurthy, M.R. Chance, R. Mendelsohn, E.P. Paschalis, F. Betts, A.L. Boskey, In situ analysis of mineral content and crystallinity in bone using infrared micro-spectroscopy of the $\nu(4)$ PO_4^{3-} vibration, Biochim. Biophys. Acta 1527 (2001) 11–19.
[33] M.E. Fleet, X. Liu, Carbonate Apatite type A synthesized at high pressure: new space group and orientation of channel carbonate ion, J. Solid State Chem. 174 (2) (2003) 412–417.
[34] M.E. Fleet, X. Liu, Location of type B carbonate ion in type A-B carbonate Apatite synthesized at high pressure, J. Solid State Chem. 177 (9) (2004) 3174–3182.
[35] N. Sahai, J.A. Tossell, Molecular orbital study of Apatite (Ca-5(PO4)(3)OH) nucleation at silica bioceramic surfaces, J. Phys. Chem. B 104 (2000) 4322–4341.
[36] B.O. Fowler, M. Markovic, W.E. Brown, Octacalcium phosphate.3. Infrared and Raman vibrational-spectra, Chem. Mater. 5 (1993) 1417.
[37] J. Xu, I.S. Butler, D.F.R. Gilson, FT-Raman and high-pressure infrared spectroscopic studies of dicalcium phosphate dihydrate ($CaHPO_4{\cdot}2H_2O$) and anhydrous dicalcium phosphate ($CaHPO_4$), Spectrochim. Acta A 55 (1999) 2801–2809.
[38] J.D. Termine, A.S. Posner, Infrared determination of the percentage of crystallinity in Apatite calcium phosphates, Nature 211 (1966) 268–270.
[39] I.R. Gibson, S.M. Best, W. Bonfield, Chemical characterization of silicon-substituted hydroxyapatite, J. Biomed. Mater. Res. 44 (1999) 422.
[40] P.A.A.P. Marques, M.C.F. Magalhães, R.N. Correia, M. Vallet-Regi, Synthesis and characterization of silicon-substituted hydroxyapatite, Key Eng. Mater. 192 (2000) 247–250.
[41] I. Mayer, R. Schlam, F.D.B. Featherstone, Magnesium-containing carbonate Apatites, J. Inorg. Biochem. 66 (1997) 1–6.
[42] M. Aizawa, T. Terado, F.S. Howell, K. Itatani, Preparation of spherical Apatite particles by the homogeneous precipitation method in the presence of magnesium ions and their ion-exchange properties, Mater. Res. Bull. 34 (n 8) (1999) 1215–1225.
[43] E. Bertoni, A. Bigi, G. Cojazzi, M. Gandolfi, S. Panzavolta, N. Roveri, Nanocrystals of magnesium and fluoride substituted hydroxyapatite, J. Inorg. Biochem. 72 (1998) 29–35.
[44] S.R. Kim, J.H. Lee, Y.T. Kim, D.H. Riu, S.J. Jung, Y.J. Lee, S.C. Chung, Y.H. Kim, Synthesis of Si, Mg substituted hydroxyapatites and their sintering behaviours, Biomaterials 24 (8) (2003) 1389–1398.
[45] C. Gaillard, N. Chevarier, C. Den Auwer, N. Millard-Pinard, P. Delichere, P. Sainsot, Study of mechanisms involved in thermal migration of molybdenum and rhenium in Apatites, J. Nucl. Mater. 299 (2001) 43–52.
[46] X.L. Tang, X.F. Xiao, R.F. Liu, Structural characterization of silicon-substituted hydroxyapatite synthesized by a hydrothermal method, Mater. Lett. 59 (2005) 3841–3846.
[47] M. Wakamura, K. Kandori, T. Ishikawa, Surface structure and composition of calcium hydroxyapatites substituted with Al(III), La(III) and Fe(III) ions, Colloids Surf., A 164 (2000) 297–305.
[48] T.L. Hughes, C.M. Methven, T.G.J. Jones, S.E. Pelham, P. Fletcher, C. Hall, Determining cement composition by Fourier transform infrared spectroscopy, Adv. Cem. Based Mater. 2 (1995) 91–104.
[49] M. D'Apuzzo, A. Aronne, S. Esposito, P. Pernice, Sol-gel synthesis of humidity-sensitive P_2O_5-SiO_2 amorphous films, J. Sol-Gel Sci. Technol. 17 (2000) 247–254.